Contents lists available at ScienceDirect

Extreme Mechanics Letters

journal homepage: www.elsevier.com/locate/eml



Enhancement of hydrodynamic friction by periodic variation of contact stiffness



Haibin Wu^a, Constantine Khripin^d, Anand Jagota^c, Chung-Yuen Hui^{a,b,*}

- ^a Department of Mechanical and Aerospace Engineering, Field of Theoretical and Applied Mechanics, Cornell University, Ithaca, NY 14853, USA
- ^b Global Station for Soft Matter, GI-CoRE, Hokkaido University, Sapporo, Japan
- ^c Departments of Bioengineering and of Chemical & Biomolecular Engineering, 111 Research Drive, Lehigh University, Bethlehem, PA 18015, USA
- d Michelin Americas Research Center, 515 Michelin Road, Greenville, SC 29605, USA

ARTICLE INFO

Article history: Received 27 September 2021 Accepted 6 April 2022 Available online 11 April 2022

Keywords: Transient elasto-hydrodynamics Lubrication Hydrodynamic friction Structured surface

ABSTRACT

A common way to increase friction during lubricated sliding is to increase energy dissipation in the slider or the substrate, for example, by bulk viscoelasticity. It has recently been shown that lubricated friction can also be enhanced by surface architecture, specifically by periodic variation of near-surface stiffness. We study this phenomenon by considering a rigid cylinder undergoing lubricated sliding on a substrate with a periodic variation in mechanical stiffness. We model the process using the Reynolds theory for transient elasto-hydrodynamic lubrication (t-EHL). We developed a numerical scheme to solve this t-EHL problem and used it to study how surface variation in stiffness affects the motion of the cylinder, the distribution of hydrodynamic pressure, the liquid film thickness, and the friction force. Our results indicate that increasing the variation of the near-surface stiffness can significantly increase the friction force. The numerical method developed in this work can be applied to other transient EHL problems with slight modification. Our results provide insight into the mechanism of friction enhancement and can guide design of surfaces to control friction during lubricated sliding.

© 2022 Elsevier Ltd. All rights reserved.

1. Introduction

Lubrication is ubiquitous, it occurs in scenarios as disparate as synovial joints, and between eyes and their lids/eyes in soft living matter to power-transmitting components in motor vehicles. Lubricated elastic contacts have been extensively studied [1-3] with a heavy emphasis on metal contacts such as bearings [4,5] and pistons [6,7]. For more compliant materials the effect of deformations on the contact geometry and pressure profile, as well as hysteretic friction forces need be considered [8-12]. Depending on the sliding velocity and the normal load, lubrication can be divided into elasto-hydrodynamic lubrication (EHL), mixed, and boundary lubrication regimes [13,14]. Our interest in this work is confined to the EHL regime, where there is no solid-solid contact between the lubricated surfaces. Within the EHL regime, we may further distinguish steady-state EHL (s-EHL) and transient EHL (t-EHL) sliding problems depending on whether the solution is a function of time.

More importantly, surface texture, such as artificial microgrooves or micro-dimples fabricated on the contact surface, has

E-mail address: ch45@cornell.edu (C.-Y. Hui).

been proven to be effective at modulating the tribological performance [15-24]. However, there is relatively little research on the use of surface architecture to control the lubricated contact and sliding behavior of a soft solid on a hard surface. In a recent work [25,26], we have shown experimentally that periodic variation in near-surface stiffness of a soft substrate can significantly enhance lubricated friction in the EHL regime. We proposed that the additional energy loss came from mechanical energy loss as the indenter moved from the stiff to the soft region. Our interest in this work is to model this phenomenon. The problem is a difficult one, since even though the cylinder is moving at a fixed velocity, the steady state assumption breaks down due to variation of surface stiffness. To tackle this problem, we develop a t-EHL model to study lubricated sliding of a rigid cylinder on flat inhomogeneous substrate with a sinusoidal stiffness profile. Within this setting, we explore how friction can be enhanced due to surface variation in stiffness.

Both the s-EHL and t-EHL problems are usually studied using the lubrication theory developed by Reynolds [27]. Most previous EHL sliding studies focused on examining the s-EHL problems with a cylinder-on-flat or sphere-on-flat contact geometry to investigate the effects of properties such as material modulus, lubricant viscosity, bulk viscoelasticity [28], and surface roughness [29–37]. Even for s-EHL problems, many numerical difficulties have been encountered due to the nonlinearity of the

^{*} Corresponding author at: Department of Mechanical and Aerospace Engineering, Field of Theoretical and Applied Mechanics, Cornell University, Ithaca, NY 14853, USA.

Fig. 1. A schematic of lubricated sliding of a rigid cylinder on a patterned elastic foundation.

governing equations, especially in the so-called Hertz limit, in which a large normal load is applied to the indenter which results in the fluid layer being much thinner than the deformation of the soft solid [38–40]. Many techniques have been proposed to overcome these numerical difficulties, such as the inverse method introduced by Dowson and Higginson [41] for the line load steady EHL problems; a robust forward iteration method proposed by Hamrock and Dowson [42–45] to solve the problem of lubricated sliding of a rigid *sphere* on an infinite elastic substrate; a differential deflection method proposed by Hughes and Evan et al. [29–31] to efficiently solve the deformation of the substrate; a multintegration technique developed by Lubrecht and Brandt [46] to accelerate the calculation of the substrate deformation; and a revised forward iteration scheme with incremental steps to approach heavy loading condition [40].

While in previous studies significant efforts were spent on improving the accuracy and efficiency of the solution of s-EHL problems, few studies have focused on the t-EHL problems and their applications. These applications include the hydrodynamic rod seal [47-49], cam-follower contact [50-52], and roller bearings [53,54]. Other research, for example the work of Wang and Frechette [55,56], also utilize t-EHL to study transient phenomena such as interaction between a particle and an elastic wall. In such applications the s-EHL models are usually inapplicable, mainly because these dynamic systems usually operate inherently in an unsteady situation where fluid squeeze effects occur. Vichard [57] studied a transient hydrodynamic lubrication problem without considering the deformation of the substrate to explore the influence of variation of the parameters of the contact with time, such as the normal load applied to the cylinders, the relative radius of curvature of the cylinder, the rolling speeds and the inlet viscosity of the lubricant. Patir and Cheng [58] utilized an averaged Reynolds equation model to study the effect of surface roughness on partially lubricated contact. However, the deformation of the roughness was not taken into account in the study. Ai and Yu [51,59] combined Newton-Raphson scheme and low relaxation iteration method to study the transient process of a cam tappet to a limited accuracy. Other following works deal with transient EHL problems in different physical settings [15,60, 61]. However, most of these studies either do not consider the deformation of the substrate or the surface's roughness, or the calculation is slow and the accuracy is limited due to the lack of a fast and stable algorithm to tackle the full t-EHL problem. Therefore, there is significant need for a t-EHL model.

In this paper, we mainly focus on the hydrodynamic friction enhancement due to variation of surface stiffness in the t-EHL. The plan for this paper is as follows: Section 2 summarizes the t-EHL formulation, after which the focus shifts to numerical implementation. Section 3 presents the numerical results and comparison with the experimental data. We conclude with a summary and discussion in Section 4.

2. Governing equations of t-EHL problem

Fig. 1 shows the schematics of our problem. A rigid circular cylinder of radius R slides on an elastic substrate. The cylinder moves with a constant velocity V in the positive X direction. Here (X,Y,Z) is a Cartesian frame fixed to the substrate. The cylinder is infinitely long in the out-of-plane Y direction; the solution is independent of Y. The substrate is modeled as a spring foundation where the springs have periodic stiffness in the X direction. In the following, this periodicity is model by a sinusoidal function with period L. A thin liquid layer lubricates the foundation surface. A constant normal force N (per unit length) is imposed on the cylinder.

We also attach a moving coordinate system (x, z = Z) which is fixed to the center of the cylinder, where x = X - Vt. The displacement w(x, t) of the foundation and the surface profile of the cylinder h(x, t) are measured with respect to z = 0. Specifically, the displacement of the substrate is zero at z = 0 far away from the origin where the fluid pressure vanishes. The indentation depth is $h(x = 0, t) \equiv h_0(t)$. Since most of the pressure is confined to a region that is much smaller than R, h(x, t) is approximated as a parabola:

$$h(x,t) = h_0(t) + \frac{x^2}{2R}$$
 (1)

The transient Reynolds equation in the moving frame is (derivation is given in SI):

$$\left(\frac{p_{,x}u^3}{12\eta}\right)_{,x} = -\left(\frac{v}{2}\right)u_{,x} + u_{,t} \tag{2}$$

where "," denotes partial differentiation, p is the hydrodynamic pressure, η is the fluid viscosity and

$$u(x,t) = h(x,t) - w(x,t),$$
 (3)

is the liquid film thickness. We normalize the stiffness of the foundation k by k_0 which is the average stiffness $\frac{1}{L} \int_0^L k(X) dX$. In the moving frame, the normalized stiffness is

$$\overline{k}(x,t) \equiv \frac{k(x,t)}{k_0} = 1 + \gamma \sin \frac{2\pi}{L} (x + Vt)$$
 (4a)

where k_0 is the average stiffness and $0 \le \gamma \le 1$ is the normalized amplitude of the sinusoidal stiffness function. The deformation of the substrate w and the hydrodynamic pressure p are related by

$$p(x, t) = -k(x, t) w(x, t) = -k_0 \overline{k}(x, t) w(x, t)$$
 (4b)

Force balance requires

$$\int_{-\infty}^{\infty} p dx = N \tag{5}$$

Recall that N is fixed during sliding. Our main interest is the "long-time" solution in which all field quantities vary periodically in time.

2.1. Initial and boundary conditions

The boundary condition is

$$p(x \to \pm \infty, t) = 0. \tag{6}$$

Physically, we expect that the long-time solution will be insensitive to the initial conditions and depend only on the stiffness profile. In the following, we chose the initial pressure profile as the steady state solution of a *spatially homogeneous* foundation with stiffness k_0 (see below).

2.2. Normalization

We introduce the following normalization to simplify the analysis. The length scale we use to normalize the spatial coordinate, x, is the Hertz contact length a. Physically, a is the half width of the contact zone when a rigid cylinder of radius R is pushed vertically (without sliding) into an elastic foundation of stiffness k_0 by a normal force N [62]:

$$\bar{x} = \frac{x}{a}, \quad a \equiv \left(\frac{3NR}{2k_0}\right)^{1/3}$$
 (7a,b)

We normalize the displacement w, the cylinder's position h and the film thickness u by the indentation depth in Hertz contact, $\delta=a^2/2R$. The hydrodynamic pressure is normalized by the characteristic pressure for given indentation depth, i.e., $k_0a^2/2R$. Time is normalized by the time it takes to slide a distance a. These result in

$$\overline{w}, \overline{h}, \overline{u} = \frac{w, h, u}{a^2/2R}, \quad \overline{p} = \frac{p}{k_0 a^2/2R}, \quad t = \frac{a}{V}\overline{t}$$
 (7c-e)

After normalization, Eqs. (2)–(5) become:

$$\beta\left(\overline{p}_{,\overline{x}}\overline{u}^{3}\right)_{,\overline{x}} = -\frac{1}{2}\overline{u}_{,\overline{x}} + \overline{u}_{,\overline{t}}, \quad \overline{u} = \overline{h} - \overline{w}, \quad \overline{h}\left(\overline{x},\overline{t}\right) = \overline{h}_{0}\left(\overline{t}\right) + \overline{x}^{2}$$
(8a)

$$\overline{p} = -\overline{w}\overline{k}, \overline{k} = \overline{k}\left(\overline{x}, \overline{t}\right) = 1 + \gamma \sin\frac{2\pi}{\omega}\left(\overline{x} + \overline{t}\right) \tag{8b}$$

$$\int_{-\infty}^{\infty} \overline{p} d\overline{x} = \frac{4}{3} \tag{8c}$$

where

$$\beta = \frac{k_0 a^5}{96V \eta R^3} = (3/2)^{5/3} \frac{\left(k_0 R^2\right)^{-2/3} N^{5/3}}{96 \eta V} \tag{8d}$$

$$\omega = L/a \tag{8e}$$

Thus, the solution of our sliding problem is governed by three dimensionless parameters β , ω and γ . The constant $1/\beta$ is the generalization of the Hersey number [63] and is a normalized velocity. It is the ratio of the sliding velocity to a characteristic velocity of fluid flow at a given indentation depth. The parameter ω is the normalized wavelength of the sinusoidal stiffness; it is inversely proportional to the number of wavelengths inside the contact zone (see Fig. 2). γ is the normalized amplitude of the periodic stiffness variation; $\gamma=0$ corresponds to a substrate with no stiffness variation.

2.3. Steady state solution for an unstructured surface ($\gamma = 0$)

The initial pressure profile is set to be the steady state solution for a foundation with a uniform stiffness $k(x, t) = k_0$. For this case, the steady state solution is *independent* of time and Eq. (8a) can be solved by integrating once, resulting in

$$\beta \overline{p}_{,\overline{x}} (\overline{h} + \overline{p})^{3} = -\frac{1}{2} (\overline{h} + \overline{p}) + C(\beta), \qquad \overline{h}(\overline{x}) = \overline{h}_{0} + \overline{x}^{2}$$
 (9)

where $\overline{h}_0(\beta)$ and $C(\beta)$ are unknown constants determined by force balance Eq. (7c) and the boundary condition $p(x \to \pm \infty) = 0$. Eq. (9) can be solved using an ODE solver. In a previous work, we have shown that for large β , $C(\beta) = c_0 \beta^{-1/2}$ where $c_0 = 1/\sqrt{26}$ (see [64] for more details). For large β , the pressure distribution is well approximated by the Hertz pressure:

$$\overline{p} = 1 - \overline{x}^2, \quad |\overline{x}| < 1 \tag{10}$$

2.4. Numerical scheme

Due to periodic variation of stiffness, the long-time pressure distribution is periodic but still time dependent. Here we use a finite difference method to solve the transient EHL equation. The spatial derivatives are approximated using central differences:

$$\bar{p}_{,\bar{x}} = \frac{\bar{p}_{i+1}^{(k)} - \bar{p}_{i-1}^{(k)}}{2\Delta\bar{x}}, \quad \bar{u}_{,\bar{x}} = \frac{\bar{u}_{i+1}^{(k)} - \bar{u}_{i-1}^{(k)}}{2\Delta\bar{x}},
\bar{p}_{,\bar{x}\bar{x}} = \frac{\bar{p}_{i+1}^{(k)} - 2\bar{p}_{i}^{(k)} + \bar{p}_{i-1}^{(k)}}{(\Delta\bar{x})^{2}}$$
(11)

where the superscript k represents time step \overline{t}_k and subscripts i-1,i,i+1 denote positions x_{i-1},x_i,x_{i+1} . We use a uniform mesh so $\Delta \overline{x}=\overline{x}_{i+1}-\overline{x}_i$ for $1\leq i\leq n$ where n is the total number of nodes in the calculation domain $\overline{x}\in[-5,5]$. At the boundary $\overline{x}=\pm 5, i=1,n$, we enforced the boundary conditions $\overline{u}=0, \overline{p}=\overline{p}, \overline{x}=0$ and $\overline{u}, \overline{x}=0, \overline{p}=\overline{p}, \overline{x}=0$. We use backward scheme to compute the time derivative, i.e.,

$$\overline{u}_{,\overline{t}}^{(k)} = \frac{\overline{u}_{i}^{(k)} - \overline{u}_{i}^{(k-1)}}{\Lambda \overline{t}}$$
 (12)

Using Eqs. (11)–(12), the discretized transient Reynold equation Eqs. (8a)–(8b) becomes:

$$\underbrace{\left[\frac{\left(\overline{u}_{i}^{(k)}\right)^{2}}{\left(\Delta\overline{x}\right)^{2}}\left(\frac{3}{4}\overline{u}_{i-1}^{(k)} + \overline{u}_{i}^{(k)} - \frac{3}{4}\overline{u}_{i+1}^{(k)}\right)\right]}_{A_{i}}\overline{p}_{i-1}^{(k)} + \underbrace{\left(-2\frac{\left(\overline{u}_{i}^{(k)}\right)^{3}}{\left(\Delta\overline{x}\right)^{2}} - \frac{1}{\beta\Delta\overline{t}\cdot f_{i}^{(k)}}\right)}_{B_{i}}\overline{p}_{i}^{(k)} + \underbrace{\left[\frac{\left(\overline{u}_{i}^{(k)}\right)^{2}}{\left(\Delta\overline{x}\right)^{2}}\left(-\frac{3}{4}\overline{u}_{i-1}^{(k)} + \overline{u}_{i}^{(k)} + \frac{3}{4}\overline{u}_{i+1}^{(k)}\right)\right]}_{B_{i}}\overline{p}_{i+1}^{(k)} + \underbrace{\frac{1}{\beta}\left(-\frac{\overline{u}_{i+1}^{(k)} - \overline{u}_{i-1}^{(k)}}{4\Delta\overline{x}} + \frac{d\overline{h}_{0}^{(k)}}{d\overline{t}} - \frac{\overline{p}_{i}^{(k-1)}}{\Delta\overline{t}\cdot f_{i}^{(k-1)}}\right)}_{D_{i}} \\ \overline{p}_{i}^{(k)} = -\overline{w}_{i}^{(k)}f_{i}^{(k)} = \left(\overline{u}_{i}^{(k)} - \overline{h}_{0}^{(k)} - \overline{x}_{i}^{2}\right)f_{i}^{(k)} \tag{13b}$$

The steady-state solution in 2.3, denoted by
$$\overline{p}^{(0)}$$
, $\overline{h}_0^{(0)}$, $\overline{u}^{(0)}$ is used as the initial condition. At time step k , we use the solution at the previous time step $(k-1)$ and guess the cylinder's vertical position $\overline{h}_0^{(k)}$ to determine $d\overline{h}_0^{(k)}/d\overline{t} \approx \left(\overline{h}_0^{(k)} - \overline{h}_0^{(k-1)}\right)/\Delta \overline{t}$. This derivative, together with the solution at the $k-1$ step, completely determines last two terms on the right hand side (RHS) of Eq. (13a), so Eqs. (13a), (13b) become an implicit nonlinear equation of $\overline{p}_{i-1}^{(k)}$, $\overline{p}_{i}^{(k)}$, $\overline{p}_{i+1}^{(k)}$. A relaxation method with a forward iteration scheme is used to solve this implicit nonlinear equation. Details are given in SI.

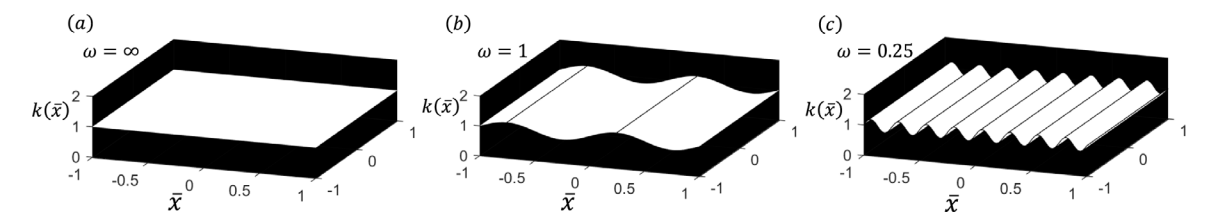


Fig. 2. Stiffness variation f of the structured surfaces: (a) homogeneous surface ($\omega = \infty$) (b) $\omega = 1$ and (c) $\omega = 0.25$. $\gamma = 0.4$ for (b) and (c).

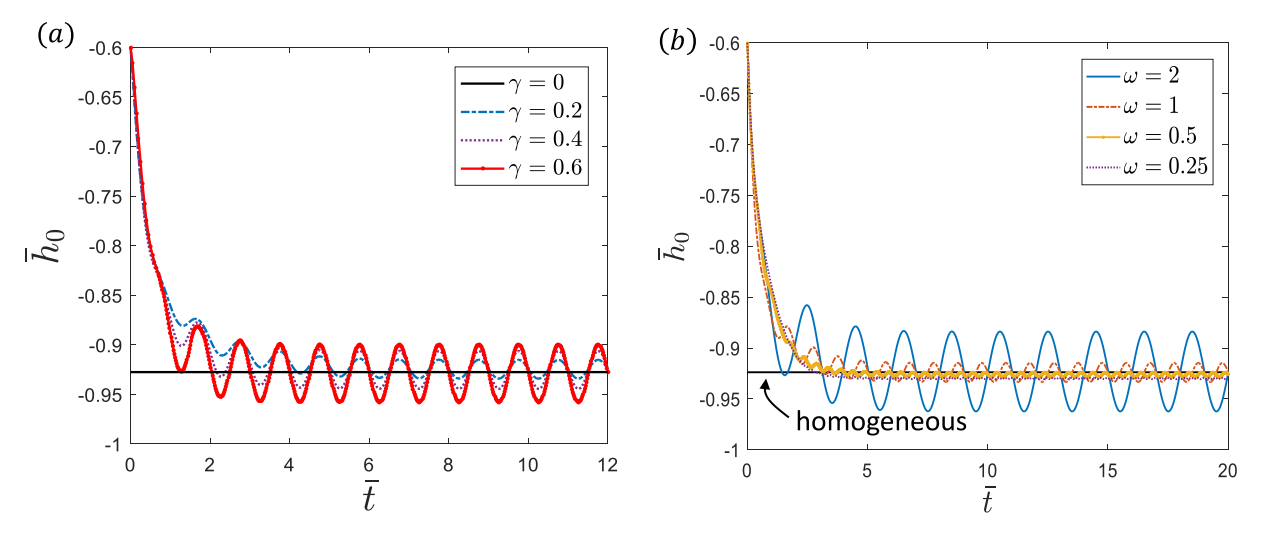


Fig. 3. Time history of indentation depth \overline{h}_0 for a cylinder sliding on surfaces structured with sinusoidal stiffness profile, (a) the sinusoidal stiffness has amplitudes $\gamma=0.0,0.2,0.4,0.6$ and $\omega=1,\beta=10$; the special case of uniform stiffness ($\gamma=0$) is the horizontal black solid line, (b) the sinusoidal stiffness has wavelengths: $\omega=0.25,0.5,1.0,2.0$ and $\gamma=0.2,\beta=10$.

3. Results and discussion

3.1. Time history of normalized cylinder indentation depth \bar{h}_0 (\bar{t})

Fig. 3 shows the time history of the indentation depth at constant normal force for $\beta=10$. The result in Fig. 3(a) is obtained using $\omega=1$ and four different amplitudes $\gamma=0.0,0.2,0.4,0.6$. The companion figure on the right, Fig. 3(b) is for $\gamma=0.2$ and four normalized wavelengths $\omega=0.25,0.5,1.0,2.0$.

Fig. 3(a,b) show that a periodic steady state is achieved for $\overline{t} = Vt/a \geq 5$, or when the indenter moves about 5a. Fig. 3(b) shows that, for a fixed ω , the vertical motion of the cylinder is periodic, the time average of \overline{h}_0 in a cycle is close to the case where the foundation is spatially homogeneous (the horizontal line). As expected, larger γ results in larger up-down motion of the cylinder. Also, for fixed γ , β , larger ω results in larger up-down motion of the cylinder. In SI, we show that, at long times, the maximum value of \overline{h}_0 plateaus to a limiting value as ω increases.

3.2. Hydrodynamic pressure and liquid film thickness

Snapshots of the pressure profiles are shown in Fig. 4 for structured surfaces with $\omega=1$, $\beta=10$ and different stiffness amplitudes γ . Our numerical results show that, for $\beta=5$, hydrodynamic pressure is practically zero outside $\overline{x}\in[-1,1]$, which justifies our use of Hertz contact length to normalize distance. For this reason, we shall call 2a the length of the contact zone even though solid-solid contact does not exist due to the presence of the liquid film. Fig. 4(a) shows that there are significant differences between the pressure profiles of the structured and the homogeneous surface with no stiffness variation (black solid line, $\gamma=0$). These differences increase with γ . Note

 $\omega=1$ implies that there is roughly one soft and one hard region within the contact zone (see Fig. 2); this explains the two pressure peaks. These peaks are located roughly near the center of each region. The maximum pressure always occurs in the hard region. As expected, the maximum and the minimum pressure increases/decreases with ν .

Fig. 4(b) plots the pressure distribution associated with different ω ($\gamma=0.2, \beta=10$). For smaller wavelengths such as $\omega=0.5$, there are multiple pressure spikes inside the contact zone. A rough estimate of the number of pressure peak is $2/\omega$. Again, the maximum and minimum pressure increase/decreases with decreasing wavelength ω .

Liquid film thickness profiles are plotted in Fig. 5(a,b) for $\beta=10$. The special case of a homogeneous surface ($\gamma=0$ or $\omega=\infty$) is also included in these figures as a comparison (solid black lines). Just like the pressure distribution, the film thickness has peaks and valleys. Since the valley corresponds to pressure peak, the number of valleys is roughly $2/\omega$. For structured surface $\gamma>0$, the minimum/maximum film thicknesses are smaller/larger than the homogeneous case and these differences increase with γ but decreases with ω .

3.3. Fluid flow velocity field

Here we provide the fluid velocity field for some structured surfaces. The normalized velocity in the moving coordinate system is related to the normalized pressure gradient by (see SI)

$$\overline{v}_{x} \equiv \frac{v_{x}}{V} = 6\beta \overline{p}_{,\overline{x}} \left(\overline{z} - \overline{h} \right) (\overline{z} - \overline{w}) + \frac{(\overline{z} - \overline{w})}{\overline{u}} - 1$$
 (14a)

Contour plots of the fluid velocity \overline{v}_x is shown in Fig. 6(a-d) for $\beta = 10$. In Fig. 6(a, b), $\omega = 1$ and $\gamma = 0.2$ and 0.4. In Fig. 6 (c, d), $\gamma = 0.2$ and $\omega = 2$ and 0.5. Due to no slip condition, the

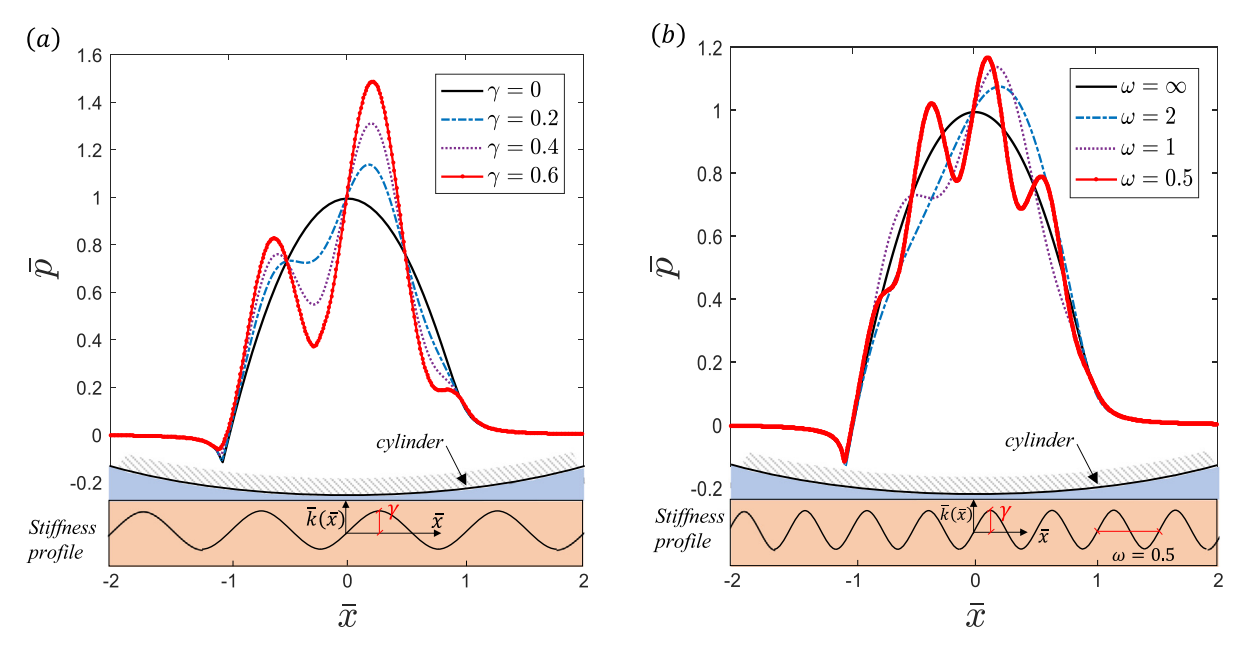


Fig. 4. Hydrodynamic pressure profile along \bar{x} on structured surfaces with different sinusoidal stiffness; (a) the sinusoidal stiffness has various amplitude $\gamma = 0, 0.2, 0.4, 0.6$ and $\omega = 1, \beta = 10, \bar{t} = 20$; (b) the sinusoidal stiffness has various wavelength $\omega = 0.5, 1, 2$ and $\gamma = 0.2, \beta = 10, \bar{t} = 20$.

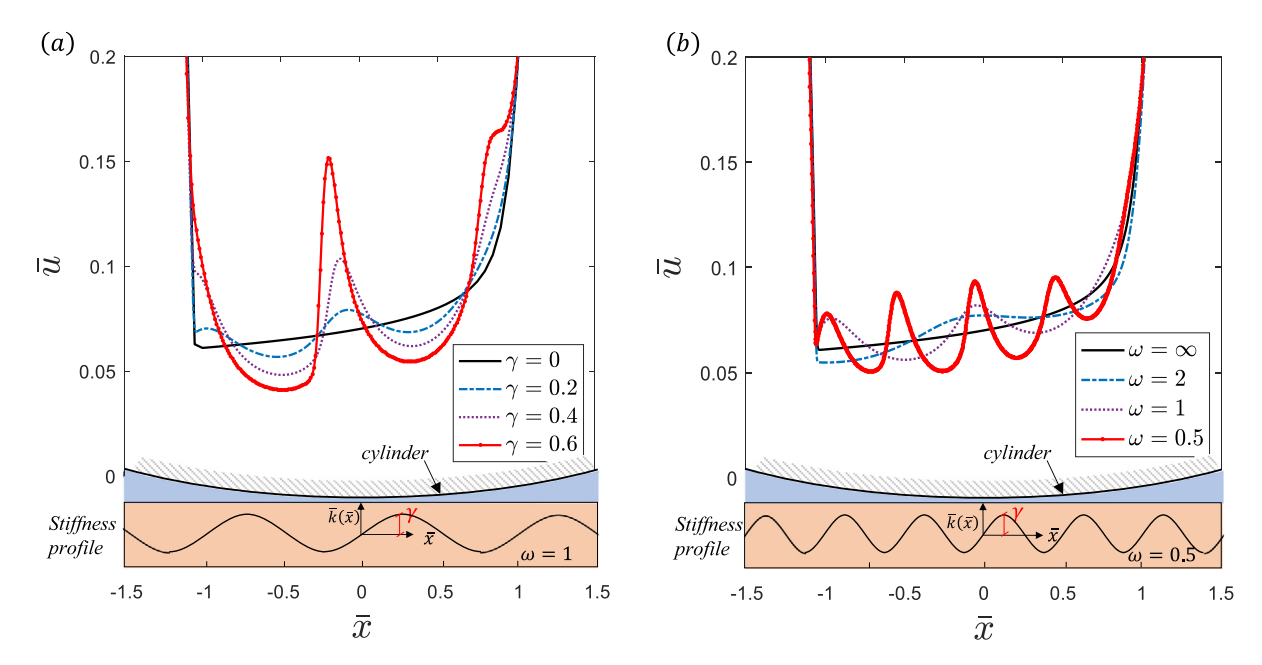


Fig. 5. Film thickness profile along \bar{x} for structured surface with different sinusoidal stiffness; (a) the sinusoidal stiffness has various amplitude $\gamma=0,0.2,0.4,0.6$ and $\omega=1,\ \beta=10,\ \bar{t}=20$; (b) the sinusoidal stiffness has various wavelength $\omega=0.5,1,2$ and $\gamma=0.2,\ \beta=10,\ \bar{t}=20$.

normalized velocity is -1 on the surface of the substrate $\overline{z}=\overline{w}$ and it is exactly 0 at the fluid/cylinder interface. In the region right in front of the cylinder (entrance), the normalized velocity component \overline{v}_x can be positive as more liquid is squeezed out. As γ increases and ω decreases, \overline{v}_x changes more rapidly across the film thickness. This is illustrated by the white dash horizontal line ($\overline{z}-\overline{w}=0.05$) in each figure.

Next, we determine the averaged velocity through the film thickness by integrating the velocity field Eq. (14a) through the film and divide it by the film thickness. After some algebra, this results in

$$\overline{v}_{x,ave} = \frac{\int_{\overline{w}}^{\overline{h}} \overline{v}_x dz}{\int_{\overline{h}}^{\overline{h}} dz} = -\beta \overline{p}_{,\overline{x}} \overline{u}^2 - \frac{1}{2}$$
 (14b)

Fig. 7 compares $\overline{v}_{x,ave}$ for patterned surface and homogeneous surface. Outside the Hertzian contact region $|\overline{x}| > 1$, the effect of surface pattern on $\overline{v}_{x,ave}$ is insignificant. However, within $|\overline{x}| \leq 1$, $\overline{v}_{x,ave}$ changes significantly. Fig. 7(a, b) show that for a fixed ω , the amplitude of $\overline{v}_{x,ave}$ increases in $|\overline{x}| \leq 1$ as γ increases from 0.2 to 0.4. Note $\overline{v}_{x,ave}$ varies much more when the indenter moves from the soft to stiff region. For this case, the average flow rate is smaller than the homogeneous case. The opposite is true when the indenter moves from the stiff to the soft region. Similar results are found when γ is fixed and ω decreases from 2 to 0.5. As ω decreases, more significant variation of $\overline{v}_{x,ave}$ is found when the indenter moves from the soft to stiff region. In the stiff region, $\overline{v}_{x,ave}$ is larger than the homogeneous case.

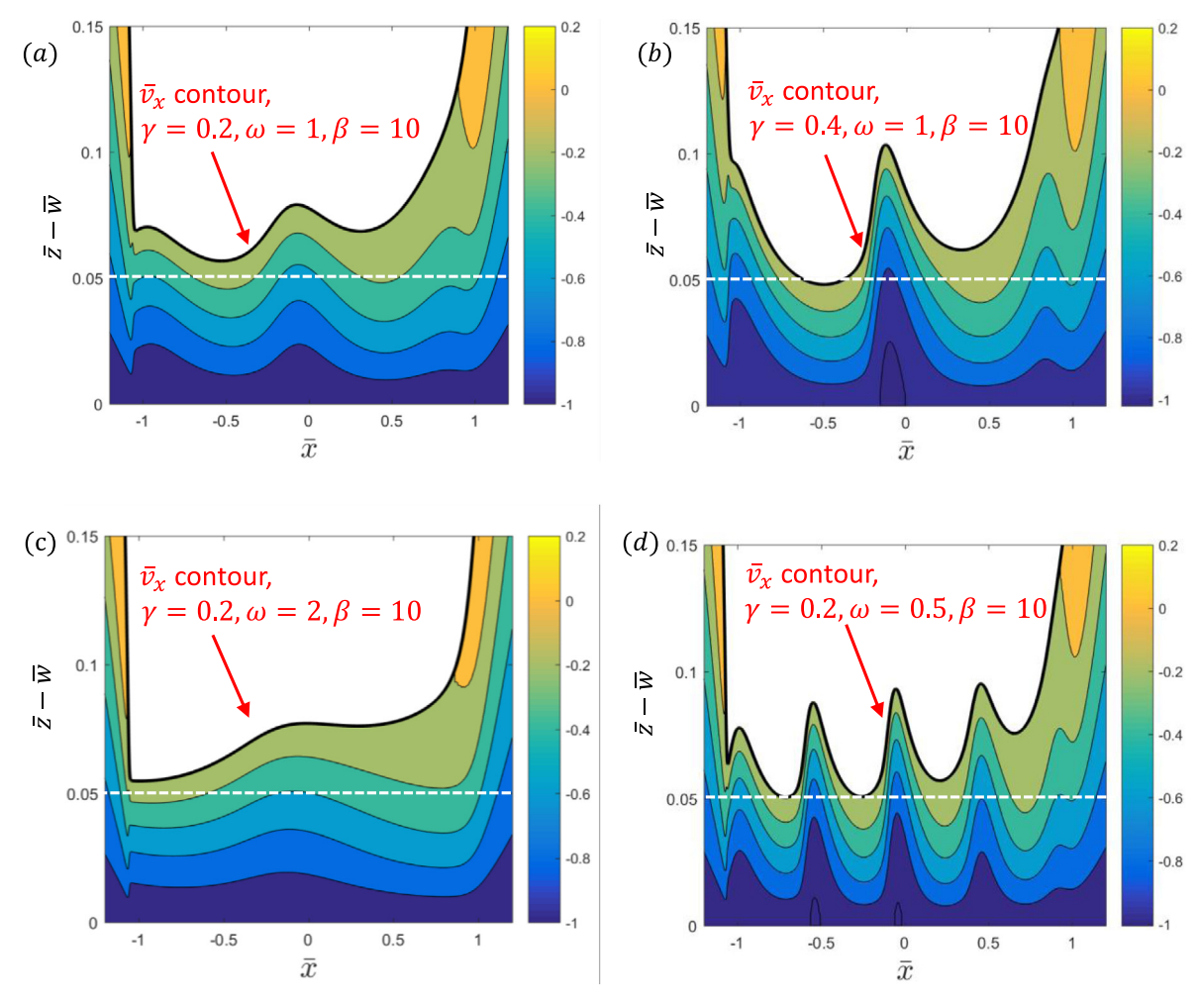


Fig. 6. Contour plot of \overline{v}_x ; (a-b) the wavelength ω of the sinusoidal stiffness profile is fixed at $\omega=1$ while the amplitude λ varies from $\gamma=0.2$ to 0.4; (c-d) $\gamma=0.2$ and ω changes from $\omega=2$ to $\omega=0.5$.

3.4. Hydrodynamic friction and friction enhancement

The shear traction τ_{zx} between the rigid cylinder and the liquid layer gives rise to a hydrodynamic friction F_f . Using Eq. (14a), the shear traction is:

$$\tau_{zx} = \eta \frac{\partial v_x}{\partial z} \Rightarrow \overline{\tau}_{zx} = \frac{\partial \overline{v}_x}{\partial \overline{z}} = 6\beta \overline{p}_{,\overline{x}} \left(2\overline{z} - \overline{h} - \overline{w} \right) + \frac{1}{\overline{u}}; \tag{15a}$$

$$\overline{\tau}_{zx}|_{\overline{z}=\overline{h}} = 6\beta \overline{p}_{,\overline{x}}\overline{u} + \frac{1}{\overline{u}}$$
 (15b)

where

$$\overline{\tau}_{zx} = \frac{a^2}{2\eta RV} \tau_{zx} = \left(\frac{3}{2\sqrt{8}}\right)^{2/3} \frac{N^{2/3}}{\eta V R^{1/3} k_0^{2/3}} \tau_{zx},\tag{15c}$$

is the normalized shear stress. The hydrodynamic friction F_f is computed by integrating the shear stress $\tau_{zx}|_{z=h}$ over $|\overline{x}|<\infty$. We define the normalized hydrodynamic friction by:

$$\overline{F}_f = \frac{a}{2R\eta V\beta} F_f = \frac{48R^2}{k_0 a^4} F_f = F_f \left[\left(\frac{3}{2} \right)^{4/3} \frac{N^{4/3}}{48R^{2/3} k_0^{1/3}} \right]^{-1}$$
 (16a)

Using Eqs. (15b), (15c), the normalized hydrodynamic friction is:

$$\overline{F}_{f} \equiv \frac{1}{\beta} \int_{-\infty}^{\infty} \overline{\tau}_{zx}|_{z=\overline{h}} d\overline{x} = \int_{-\infty}^{\infty} \left[6\overline{p}_{,\overline{x}} \left(\overline{h} - \overline{w} \right) + \frac{1}{\beta \left(\overline{h} - \overline{w} \right)} \right] d\overline{x}$$
(16b)

Time history of the normalized hydrodynamic friction \overline{F}_f is plotted in Fig. 8 for different structured surfaces. The homogeneous case $\gamma=0$ is plotted in the same figure as a comparison. The important result is that structured surface increases hydrodynamic friction. In Fig. 8(a) ($\beta=10,\omega=1$), \overline{F}_f increases with γ . For example, when $\gamma=0.2$, \overline{F}_f is slightly higher than the homogeneous case. However, \overline{F}_f is about 1.5 times of the homogeneous case when $\gamma=0.6$.

Fig. 8(b) shows that \overline{F}_f increases with the number of soft and hard regions within the contact zone (decreasing ω). The homogeneous case, $\omega=\infty$, is plotted as a reference (horizontal black line). For large $\omega\geq 2$, \overline{F}_f oscillates around the homogeneous friction (denoted by \overline{F}_f ($\omega=\infty$)). As we increase the number of soft and hard regions within a contact zone, e.g. $\omega\leq 0.5$, there is a significant increase of \overline{F}_f over \overline{F}_f ($\omega=\infty$). Specifically, when $\omega=0.25$, \overline{F}_f is $1.36\overline{F}_f$ ($\omega=\infty$).

 $\omega=0.25, \overline{F}_f$ is $1.36\overline{F}_f$ ($\omega=\infty$). The friction coefficient $\mu_f\equiv\frac{F_f}{N}=\frac{a}{24R}\frac{\overline{F}_f}{\overline{N}}$ is plotted against normalized time in Fig. 9.

To further quantify how structure changes the hydrodynamic friction, we replace the parameter γ by a new parameter $\rho \equiv k_{\min}/k_{\max}$, where k_{\max} and k_{\min} are the maximum and minimum stiffness respectively. In our model,

$$\rho \equiv k_{\min}/k_{\max} = \frac{1-\gamma}{1+\gamma} \tag{17}$$

The new parameter $\rho \in [0, 1]$; $\rho = 1$ corresponds to a homogeneous surface while $\rho = 0$ corresponds to a periodic

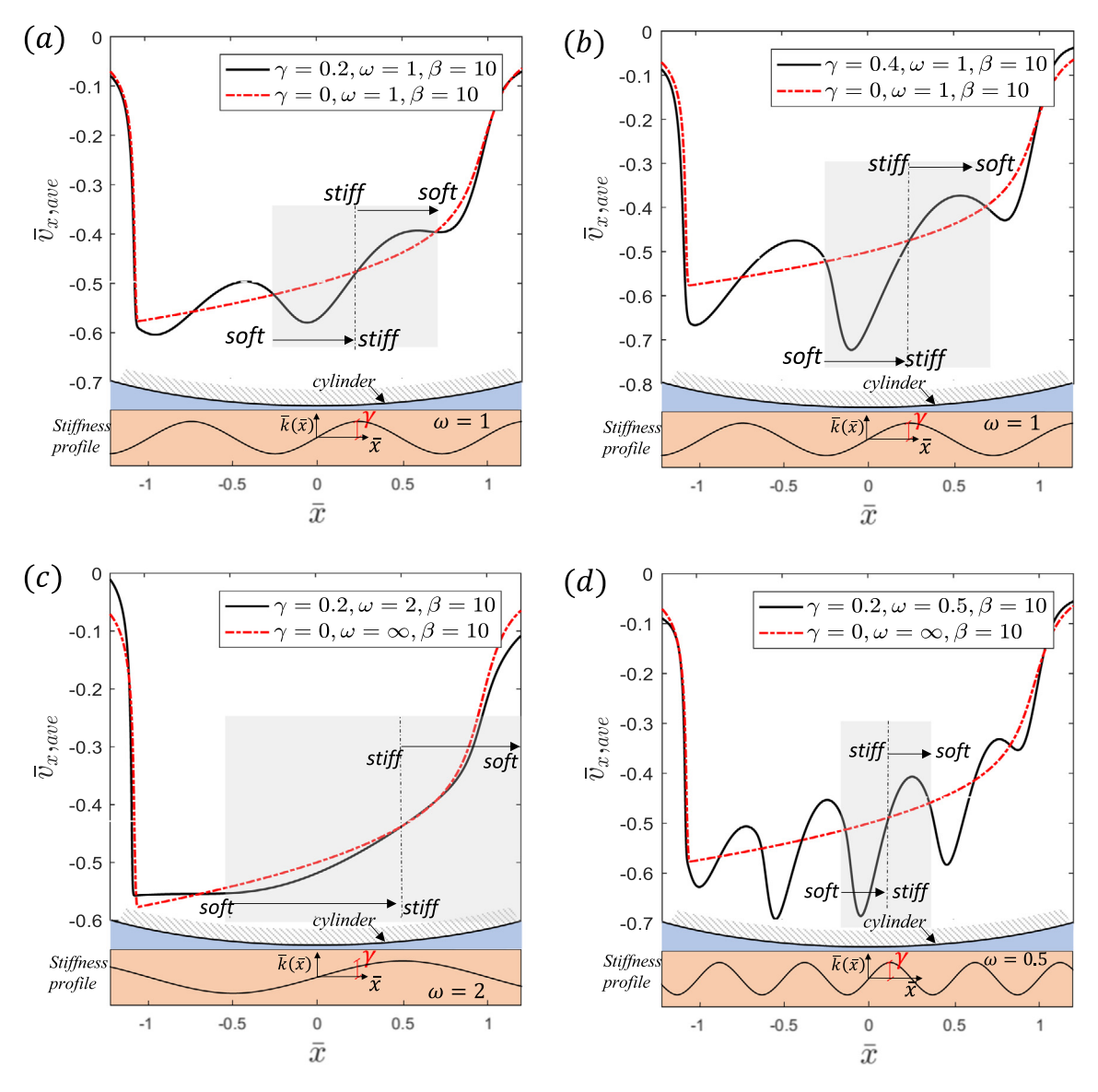


Fig. 7. Comparison of $\overline{v}_{x,ave}$ for patterned surface (black line) and homogeneous surface (red line); (a-b) the wavelength ω of the sinusoidal stiffness profile is fixed at $\omega=1$ while the amplitude λ is varied from $\gamma=0.2$ to 0.4; (c-d) γ is fixed as $\gamma=0.2$ and ω is changed from $\omega=2$ to $\omega=0.5$. (For interpretation of the references to color in this figure legend, the reader is referred to the web version of this article.)

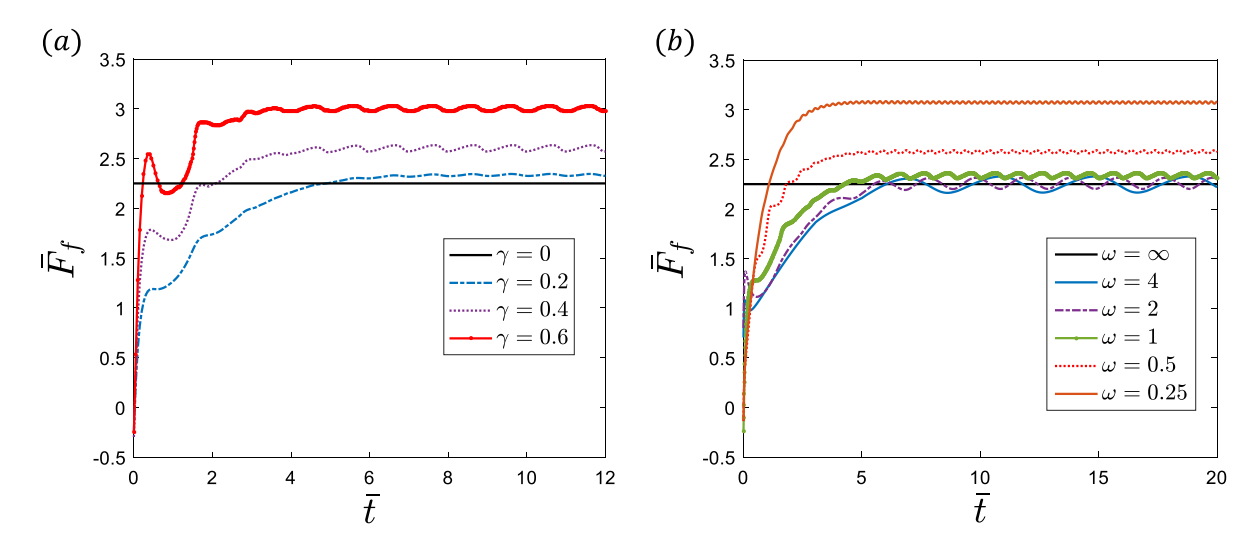


Fig. 8. Time history of the normalized hydrodynamic friction \overline{F}_f for different structured surface; (a) the structure has sinusoidal stiffness with different amplitude $\gamma=0,0.2,0.4,0.6$ ($\omega=1,\beta=10$); (b) the structure has sinusoidal stiffness with different $\omega=4,2,1,0.5,0.25$, ($\gamma=0.2,\beta=10$).

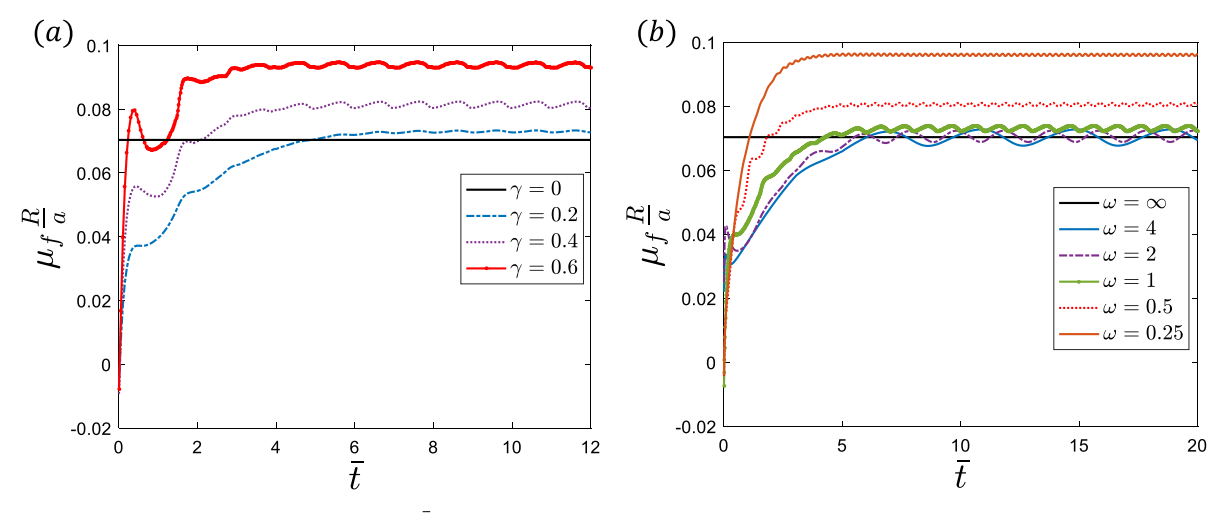


Fig. 9. Time history of the friction coefficient $\mu_f R/a = \frac{\overline{F}_f}{\overline{N}}$ for different structured surface; (a) the structure has sinusoidal stiffness with different amplitude $\gamma = 0, 0.2, 0.4, 0.6$ ($\omega = 1, \beta = 10$); (b) the structure has sinusoidal stiffness with $\omega = 4, 2, 1, 0.5, 0.25$ and $\gamma = 0.2, \beta = 10$.

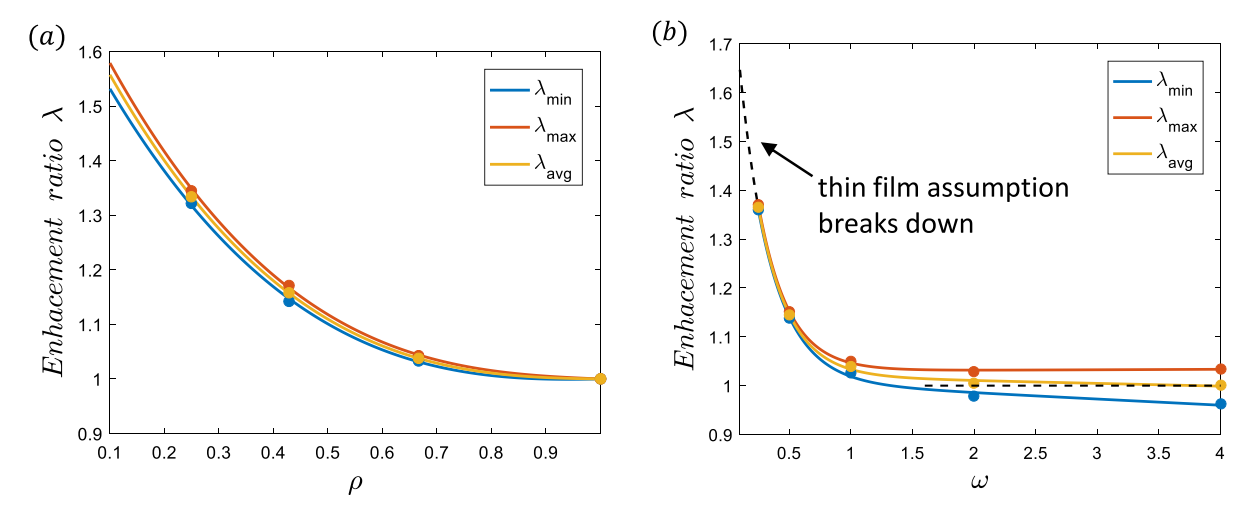


Fig. 10. Enhancement ratio versus two parameters: (a) ρ with $\omega = 1$, $\beta = 10$; (b) ω with $\rho = 2/3$, $\beta = 10$.

surface modulated by very soft and very hard regions. We measured enhancement of hydrodynamic friction by introducing a dimensionless parameter λ : the friction enhancement ratio:

$$\lambda = F_{f,\text{structured}}/F_{f,\text{homogeneous}} = \overline{F}_{f,\text{structured}}/\overline{F}_{f,\text{homogeneous}}$$
 (18a)

Since the hydrodynamic friction oscillates, we define three related quantities:

$$\begin{split} \lambda_{\text{max}} &= \frac{\text{max}\left(\overline{F}_{f,\text{structured}}\right)}{\overline{F}_{f,\text{homogeneous}}}; \lambda_{\text{min}} = \frac{\text{min}\left(\overline{F}_{f,\text{structured}}\right)}{\overline{F}_{f,\text{homogeneous}}}; \\ \lambda_{avg} &= \frac{\int_{0}^{\omega} \overline{F}_{f,\text{structured}} d\omega}{\overline{F}_{f,\text{homogeneous}}} \end{split} \tag{18b-d}$$

where: $\overline{F}_{f,\text{structured}}$ is \overline{F}_f for a structured surface and $\overline{F}_{f,\text{homogeneous}}$ corresponds to a homogeneous surface.

These friction enhancement ratios are plotted against ρ and ω in Fig. 10a,b. Fig. 10(a) shows that for $\omega=1$, the enhancement ratio increases with decreasing ρ . This figure shows that as $\rho \to 1$ (homogeneous surface) there is no hydrodynamic friction enhancement. The enhancement ratio can exceed 1.5. In Fig. 10(b) the enhancement ratio λ increases with decreasing ω . For $\omega \geq 4$, there is hardly any hydrodynamic friction enhancement. Significant enhancement of friction is achieved at $\omega=0.25$. However, one should note that further decreasing ω will not achieve more

enhancement. In our model, the ratio of the minimum liquid film thickness over the surface structure wavelength is $u_{\min}/L = \overline{u}_{\min}a/\left(2\omega R\right)$. For $\omega=0.1$, $\overline{u}_{\min}\approx0.04$ and $u_{\min}/L\approx0.2a/R$. Further decreasing ω would eventually make u_{\min}/L so large that the thin film assumption of Reynold's theory breaks down. In the limit of $\omega\to0$, the size of the feature is vanishingly small in comparison with the size of the contact zone, hence the surface behaves as a homogeneous surface with average stiffness k0 and there should be no friction enhancement.

3.5. Effect of β on film thickness \overline{u} and hydrodynamic friction \overline{F}_f

Larger β corresponds to larger normal force and smaller sliding velocity. Our numerical results reveal scaling behavior between friction and sliding rate. The results are shown in Fig. 11. For the homogeneous surface, we have shown in previous work that $\overline{F}_f \propto \beta^{-1/2}$ for $\beta \geq 10$ [64]. For structured surfaces, our result show that $\overline{F}_f \propto \beta^{-b}$, where b is a constant depending on γ and ω . For structured surface with $\omega=1$, the power law exponent b varies between 0.42 and 0.43 for $\gamma=0$ to $\gamma=0.4$ (or $\rho\in[0.428,1]$) . We also studied the effect of β on film thickness \overline{u} and hydrodynamic friction enhancement ratio λ_{avg} . More details could be found in SI.

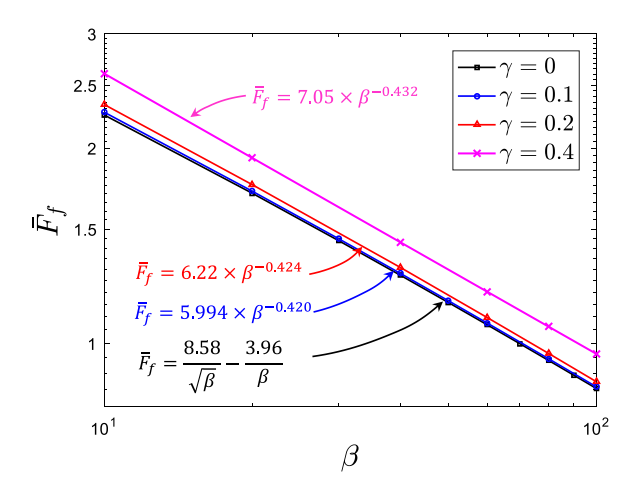


Fig. 11. Normalized hydrodynamic friction \overline{F}_f versus β for structured surface $(\omega=1)$ with different stiffness amplitude. The homogeneous case is the black line.

4. Summary and discussion

In this paper, we focused on a special case of a transient elastohydrodynamic lubrication problem: lubricated sliding of a rigid cylinder on an elastic foundation with sinusoidal stiffness profile. Enhancement of friction in hydrodynamic lubrication is conventionally thought to come mainly from the substrate's deformation and associated energy dissipation, for example, due to viscoelasticity. We have recently shown experimentally that enhancement of hydrodynamic lubrication friction can also come from surface architecture. In this work we develop a model and a new numerical scheme to explain this phenomenon. This numerical scheme allows us to study the time dependent hydrodynamic pressure profile, fluid film thickness as well as the velocity field during sliding. We focus on thin elastic substrates for which the elastic foundation model is a very good approximation. We found that when the elastic foundations are patterned with a sinusoidal stiffness profile, lubricated sliding of a rigid cylinder on this substrate exhibits a significant improvement of hydrodynamic friction F_f . This is due to that these patterned stiffness in the structured surface locally changes the liquid film thickness as well as the pressure gradient, which ultimately affects hydro-shearing force and bring more hydrodynamic friction. To develop a physical understanding of why spatial variation in contact stiffness leads to increase in dissipation, consider a much simpler problem of Couette flow between two parallel planes, one rigid and the other a spring foundation with varying contact stiffness. As $\gamma \to 0$, we have simple Couette flow given by equation S.9a in SI. There is no pressure gradient and only the second term, corresponding to Couette flow survives. Its derivative with respect to z gives the shear force, which results in friction. As γ take on a small value, this sets up a variation in film thickness, which results in a periodic pressure gradient. This, in turn, activates the Poiseuille flow (first term in S.9a in SI). For this term at z = h, it has the product of pressure gradient and (h-w) both of which will vary sinusoidally. As a result, their product adds a positive term to the shear deformation rate. This corresponds to the vertical pumping action on the fluid layer due to spatially varying contact stiffness that was introduced in [25]. Specifically, our result show that significant enhancement of friction occurs for surfaces with shorter wavelength and larger amplitude. We also discovered interesting scaling relationship between friction and velocity for different structural surfaces.

With little modification, the numerical formulations and schemes presented in this work can be used to simulate other transient EHL problems. The results presented here could serve as a guideline for designing special surfaces to improve hydrodynamic friction performances.

Declaration of competing interest

The authors declare that they have no known competing financial interests or personal relationships that could have appeared to influence the work reported in this paper.

Acknowledgments

This work was supported by the National Science Foundation, USA, through a LEAP-HI/GOALI grant, CMMI-1854572.

Appendix A. Supplementary data

Supplementary material related to this article can be found online at https://doi.org/10.1016/j.eml.2022.101735.

References

- [1] A. (Alastair) Cameron, Basic Lubrication Theory, E. Horwood, 1976.
- [2] D. Dowson, G.R. Higginson, J.F. Archard, A.W. Crook, Elasto-Hydrodynamic Lubrication, Pergamon Press, 1977.
- [3] B.N.J. Persson, Sliding Friction, Physical Principles and Applications, second ed., Springer-Verlag, 2000.
- [4] E.H. Okrent, The effect of lubricant viscosity and composition on engine friction and bearing wear, ASLE Trans. 4 (1961) 97–108, http://dx.doi.org/ 10.1080/05698196108972423
- [5] S.T. Tzeng, E. Saibel, Surface roughness effect on slider bearing lubrication, ASLE Trans. 10 (1967) 334–348, http://dx.doi.org/10.1080/ 05698196708972191.
- [6] B.L.S. Martz, Preliminary report of developments in interrupted surface finishes, Proc. Inst. Mech. Eng. 16 (1947) 1–9, http://dx.doi.org/10.1111/j. 1559-3584.1950.tb02844.x.
- [7] J.A. Mcgeehan, A Literature Review of the Effects of Piston and Ring Friction and Lubricating Oil Viscosity on Fuel Economy, SAE Technical Paper Series, 1978, http://dx.doi.org/10.4271/780673.
- [8] B.N.J. Persson, M. Scaraggi, On the transition from boundary lubrication to hydrodynamic lubrication insoft contacts, J. Phys. Condens. Matter. 21 (2009) 185002, http://dx.doi.org/10.1088/0953-8984/21/18/185002.
- [9] M. Scaraggi, G. Carbone, B.N.J. Persson, D. Dini, Lubrication in soft rough contacts: A novel homogenized approach. Part I - Theory, Soft Matter. 7 (2011) 10395–10406, http://dx.doi.org/10.1039/c1sm05128h.
- [10] M. Scaraggi, G. Carbone, D. Dini, Lubrication in soft rough contacts: A novel homogenized approach. Part II - discussion, Soft Matter. 7 (2011) 10407, http://dx.doi.org/10.1039/c1sm05129f.
- [11] J.M. Skotheim, L. Mahadevan, Soft lubrication: The elastohydrodynamics of nonconforming and conforming contacts, Phys. Fluids 17 (2005) 1–23, http://dx.doi.org/10.1063/1.1985467
- http://dx.doi.org/10.1063/1.1985467. [12] B. Saintyves, T. Jules, T. Salez, L. Mahadevan, Self-sustained lift and low friction via soft lubrication, Proc. Natl. Acad. Sci. USA 113 (2016)
- 5847–5849, http://dx.doi.org/10.1073/pnas.1525462113.
 [13] B. Jacobson, The stribeck memorial lecture, Tribol. Int. 36 (2003) 781–789, http://dx.doi.org/10.1016/S0301-679X(03)00094-X.
- [14] X. Lu, M.M. Khonsari, E.R.M. Gelinck, The stribeck curve: Experimental results and theoretical prediction, J. Tribol. 128 (2006) 789, http://dx.doi. org/10.1115/1.2345406.
- [15] L. Mourier, D. Mazuyer, A.A. Lubrecht, C. Donnet, Transient increase of film thickness in micro-textured EHL contacts, Tribol. Int. 39 (2006) 1745–1756, http://dx.doi.org/10.1016/j.triboint.2006.02.037.
- [16] T. Touche, J. Cayer-Barrioz, D. Mazuyer, Friction of textured surfaces in EHL and mixed lubrication: Effect of the groove topography, Tribol. Lett. 63 (2016) 25, http://dx.doi.org/10.1007/s11249-016-0713-8.
- [17] M. Suh, Y. Chae, S. Kim, T. Hinoki, A. Kohyama, Effect of geometrical parameters in micro-grooved crosshatch pattern under lubricated sliding friction, Tribol. Int. 43 (2010) 1508–1517, http://dx.doi.org/10.1016/j.triboint.2010.
- [18] H. Wu, N. Moyle, A. Jagota, C.Y. Khripin, F. Bremond, C.-Y. Hui, Crack propagation pattern and trapping mechanism of rolling a rigid cylinder on a periodically structured surface, Extreme Mech. Lett. 29 (2019) 100475, http://dx.doi.org/10.1016/j.eml.2019.100475.
- [19] N. Moyle, Z. He, H. Wu, C.-Y. Hui, A. Jagota, Indentation versus rolling: Dependence of adhesion on contact geometry for biomimetic structures, Langmuir 34 (2018) 3827–3837, http://dx.doi.org/10.1021/acs.langmuir. 8b00084.

- [20] B. Bhushan, Biomimetics: lessons from nature—an overview, Philos. Trans. R. Soc. A Math. Phys. Eng. Sci. 367 (2009) 1445–1486, http://dx.doi.org/10. 1098/rsta.2009.0011.
- [21] A. Jagota, C.-Y. Hui, Adhesion, friction, and compliance of bio-mimetic and bio-inspired structured interfaces, Mater. Sci. Eng. R Rep. (2011) http://dx.doi.org/10.1016/j.mser.2011.08.001.
- [22] G. Carbone, E. Pierro, A review of adhesion mechanisms of mushroom-shaped microstructured adhesives, Meccanica 48 (2013) 1819–1833, http://dx.doi.org/10.1007/s11012-013-9724-9.
- [23] L. Heepe, S.N. Gorb, Biologically inspired mushroom-shaped adhesive microstructures, Annu. Rev. Mater. Res. 44 (2014) 173–203, http://dx.doi. org/10.1146/annurev-matsci-062910-100458.
- [24] N. Moyle, F. Bremond, C.-Y. Hui, H. Wu, A. Jagota, C. Khripin, Material with enhanced sliding friction, in: U.S. Patent Application No. 20210283955, 2021, https://www.freepatentsonline.com/y2021/0283955.html.
- [25] N. Moyle, H. Wu, C. Khripin, F. Bremond, C.-Y. Hui, A. Jagota, Enhancement of elastohydrodynamic friction by elastic hysteresis in a periodic structure, Soft Matter. (2020) http://dx.doi.org/10.1039/C9SM02087J, 10.1039.C9SM02087J.
- [26] Nichole Moyle, Hao Dong, Haibin Wu, Constantine Khripin, Chung-yuen Hui, Anand Jagota, Increased sliding friction of a lubricated soft solid using an embedded structure, Tribol. Lett. 70 (1) (2022) 1–12, http://dx.doi.org/10.1007/s11249-021-01540-9.
- [27] I. On the theory of lubrication and its application to Mr. Beauchamp tower's experiments, including an experimental determination of the viscosity of olive oil, Proc. R. Soc. Lond. Ser. A Math. Phys. Eng. Sci. 40 (1886) 191–203, http://dx.doi.org/10.1098/rspl.1886.0021.
- [28] Haibin Wu, Anand Jagota, Hui Chung-yuen, Lubricated sliding of a rigid cylinder on a viscoelastic half space, Tribol. Lett. 70 (1) (2022) 1–17, http://dx.doi.org/10.1007/s11249-021-01537-4.
- [29] J. De Vicente, J.R. Stokes, H.A. Spikes, The frictional properties of Newtonian fluids in rolling - sliding soft-EHL contact, Tribol. Lett. 20 (2005) 273–286, http://dx.doi.org/10.1007/s11249-005-9067-3.
- [30] J.H.H. Bongaerts, K. Fourtouni, J.R. Stokes, Soft-tribology: Lubrication in a compliant PDMS-PDMS contact, Tribol. Int. 40 (2007) 1531–1542, http: //dx.doi.org/10.1016/j.triboint.2007.01.007.
- [31] C. Myant, H.A. Spikes, J.R. Stokes, Influence of load and elastic properties on the rolling and sliding friction of lubricated compliant contacts, Tribol. Int. 43 (2010) 55–63, http://dx.doi.org/10.1016/j.triboint.2009.04.034.
- [32] M. Scaraggi, G. Carbone, D. Dini, Experimental evidence of micro-EHL lubrication in rough soft contacts, Tribol. Lett. 43 (2011) 169–174, http://dx.doi.org/10.1007/s11249-011-9794-6.
- [33] J.M. Kim, F. Wolf, S.K. Baier, Effect of varying mixing ratio of PDMS on the consistency of the soft-contact stribeck curve for glycerol solutions, Tribol. Int. 89 (2015) 46–53, http://dx.doi.org/10.1016/j.triboint.2014.12.010.
- [34] S. Stupkiewicz, J. Lengiewicz, P. Sadowski, S. Kucharski, Finite deformation effects in soft elastohydrodynamic lubrication problems, Tribol. Int. 93 (2016) 511–522, http://dx.doi.org/10.1016/j.triboint.2015.03.016.
- [35] N. Selway, V. Chan, J.R. Stokes, Influence of fluid viscosity and wetting on multiscale viscoelastic lubrication in soft tribological contacts, Soft Matter. 13 (2017) 1702–1715, http://dx.doi.org/10.1039/c6sm02417c.
- [36] P. Sadowski, S. Stupkiewicz, Friction in lubricated soft-on-hard, hard-on-soft and soft-on-soft sliding contacts, Tribol. Int. 129 (2019) 246–256, http://dx.doi.org/10.1016/j.triboint.2018.08.025.
- [37] M. Rivetti, V. Bertin, T. Salez, C.-Y. Hui, C. Linne, M. Arutkin, H. Wu, E. Raphaël, O. Bäumchen, Elastocapillary levelling of thin viscous films on soft substrates, Phys. Rev. Fluids 2 (2017) 094001, http://dx.doi.org/10.1103/PhysRevFluids.2.094001.
- [38] H.P. Evans, R.W. Snidle, The elastohydrodynamic lubrication of point contacts at heavy loads, Proc. R. Soc. Lond. Ser. A Math. Phys. Eng. Sci. 382 (1982) 183–199, http://dx.doi.org/10.1098/rspa.1982.0096.
- [39] H.P. Evans, Inverse solution of Reynolds' equation of lubrication under point-contact elastohydrodynamic conditions, J. Tribol. 103 (1981) 539, http://dx.doi.org/10.1115/1.3251733.
- [40] H. Wu, N. Moyle, A. Jagota, C.-Y. Hui, Lubricated steady sliding of a rigid sphere on a soft elastic substrate: hydrodynamic friction in the hertz limit, Soft Matter. (2020) http://dx.doi.org/10.1039/C9SM02447F, 10.1039.C9SM02447F.
- [41] D. Dowson, G.R. Higginson, A numerical solution to the elasto-hydrodynamic problem, J. Mech. Eng. Sci. 1 (1959) 6–15, http://dx.doi.org/10.1243/JMES_JOUR_1959_001_004_02.
- [42] B.J. Hamrock, D. Dowson, Isothermal elastohydrodynamic lubrication of point contacts: Part 1—Theoretical formulation, J. Lubr. Technol. 98 (1976) 223, http://dx.doi.org/10.1115/1.3452801.

- [43] B.J. Hamrock, D. Dowson, Isothermal elastohydrodynamic lubrication of point contacts: Part II–Ellipticity parameter results, J. Lubr. Technol. 98 (1976) 375, http://dx.doi.org/10.1115/1.3452861.
- [44] B.J. Hamrock, D. Dowson, Isothermal elastohydrodynamic lubrication of point contacts: Part III—Fully flooded results, J. Lubr. Technol. 99 (1977) 264, http://dx.doi.org/10.1115/1.3453074.
- [45] B.J. Hamrock, D. Dowson, Isothermal elastohydrodynamic lubrication of point contacts: Part IV—Starvation results, J. Lubr. Technol. 99 (1977) 15, http://dx.doi.org/10.1115/1.3452973.
- [46] A. Brandt, A.A. Lubrecht, Multilevel matrix multiplication and fast solution of integral equations, J. Comput. Phys. 90 (1990) 348–370, http://dx.doi. org/10.1016/0021-9991(90)90171-V.
- [47] A. Thatte, R.F. Salant, Transient EHL analysis of an elastomeric hydraulic seal, Tribol. Int. 42 (2009) 1424–1432, http://dx.doi.org/10.1016/j.triboint. 2009.05.026.
- [48] A. Thatte, R.F. Salant, Elastohydrodynamic analysis of an elastomeric hydraulic rod seal during fully transient operation, J. Tribol. 131 (2009) 031501, http://dx.doi.org/10.1115/1.3139057.
- [49] G.K. Nikas, Transient elastohydrodynamic lubrication of rectangular elastomeric seals for linear hydraulic actuators, Proc. Inst. Mech. Eng. J 217 (2003) 461–473, http://dx.doi.org/10.1243/135065003322620282.
- [50] J. Raisin, N. Fillot, P. Vergne, D. Dureisseix, V. Lacour, Transient thermal elastohydrodynamic modeling of cam-follower systems: Understanding performance, Tribol. Trans. 59 (2016) 720–732, http://dx.doi.org/10.1080/ 10402004.2015.1110865.
- [51] X. Ai, H. Yu, A numerical analysis for the transient EHL process of a camtappet pair in I. C. Engine, J. Tribol. 111 (1989) 413–417, http://dx.doi.org/ 10.1115/1.3261940.
- [52] D. Dowson, C.M. Taylor, G. Zhu, A transient elastohydrodynamic lubrication analysis of a cam and follower, J. Phys. D: Appl. Phys. 25 (1992) A313-A320, http://dx.doi.org/10.1088/0022-3727/25/1A/047.
- [53] X.L. Liu, D.T. Song, P.R. Yang, On transient EHL of a skew roller subjected to a load impact in rolling bearings, KEM 739 (2017) 108–119, http://dx.doi.org/10.4028/www.scientific.net/KEM.739.108.
- [54] E. Ioannides, EHL in rolling element bearings, recent advances and the wider implications, in: Tribology Series, Elsevier, 1997, pp. 3–14, http://dx.doi.org/10.1016/S0167-8922(08)70431-0.
- [55] Y. Wang, C. Dhong, J. Frechette, Out-of-contact elastohydrodynamic deformation due to lubrication forces, Phys. Rev. Lett. 115 (2015) 248302, http://dx.doi.org/10.1103/PhysRevLett.115.248302.
- [56] Y. Wang, M.R. Tan, J. Frechette, Elastic deformation of soft coatings due to lubrication forces, Soft Matter. 13 (2017) 6718–6729, http://dx.doi.org/10. 1039/C7SM01061C.
- [57] J.P. Vichard, Transient effects in the lubrication of hertzian contacts, J. Mech. Eng. Sci. 13 (1971) 173–189, http://dx.doi.org/10.1243/JMES_JOUR_ 1971_013_030_02.
- [58] N. Patir, H.S. Cheng, An average flow model for determining effects of three-dimensional roughness on partial hydrodynamic lubrication, J. Lubr. Technol. 100 (1978) 12–17, http://dx.doi.org/10.1115/1.3453103.
- [59] X. Ai, H. Yu, A full numerical solution for general transient elastohydrodynamic line contacts and its application, Wear 121 (1988) 143–159, http://dx.doi.org/10.1016/0043-1648(88)90039-7.
- [60] D. Jalali-Vahid, H. Rahnejat, Z.M. Jin, Elastohydrodynamic solution for concentrated elliptical point contact of machine elements under combined entraining and squeeze-film motion, Proc. Inst. Mech. Eng. J 212 (1998) 401–411, http://dx.doi.org/10.1243/1350650981542218.
- [61] H. Lu, M. Berzins, C.E. Goodyer, P.K. Jimack, M. Walkley, Adaptive highorder finite element solution of transient elastohydrodynamic lubrication problems, Proc. Inst. Mech. Eng. J 220 (2006) 215–225, http://dx.doi.org/ 10.1243/13506501|ET134.
- [62] K.L. Johnson, Contact Mechanics, Cambridge University Press, Cambridge, 1985, http://dx.doi.org/10.1017/CBO9781139171731.
- [63] B.N.J. Persson, M. Scaraggi, On the transition from boundary lubrication to hydrodynamic lubrication in soft contacts, J. Phys.: Condens. Matter. 21 (2009) 185002, http://dx.doi.org/10.1088/0953-8984/21/18/185002.
- [64] C.-Y. Hui, H. Wu, A. Jagota, C. Khripin, Friction force during lubricated steady sliding of a rigid cylinder on a viscoelastic substrate, Tribol. Lett. 69 (2021) 30, http://dx.doi.org/10.1007/s11249-020-01396-5.